Rare Metal Materials and Engineering
Volume 52, Issue 12, December 2023
Available online at www.rmme.ac.cn

Science Press

Cite this article as: Cao Hui, Yang Wenle, Zhou Baocheng, et al. Effect of Twin Boundaries on Supersonic Fine Particle Bombardment of TiAl Alloys via Molecular Dynamics[J]. Rare Metal Materials and Engineering, 2023, 52(12): 4073-4085. DOI: 10.12442/j.issn.1002-185X.20230323.

ARTICLE

Effect of Twin Boundaries on Supersonic Fine Particle Bombardment of TiAl Alloys via Molecular Dynamics

Cao Hui[1,2], Yang Wenle[1], Zhou Baocheng[1], Yu Zhaoliang[1], Wang Jingqi[1], Li Haiyan[1,2], Liu Jianhui[1,2], Feng Ruicheng[1,2]

[1] School of Mechanical and Electrical Engineering, Lanzhou University of Technology, Lanzhou 730050, China; [2] Key Laboratory of Digital Manufacturing Technology and Application, Ministry of Education, Lanzhou University of Technology, Lanzhou 730050, China

Abstract: TiAl alloys have become one of the most promising high-temperature lightweight structural materials in aerospace and other fields because of low density, high specific strength, high-temperature oxidation resistance and other properties. However, due to the brittleness of them, it is easy to introduce micro-cracks, holes and other defects in the forming process, which seriously affect the mechanical properties. For this reason, supersonic fine particle bombardment (SFPB), one of the surface modification techniques, was used to investigate the effect of twin boundaries (TBs) on the mechanical properties and deformation behaviour of TiAl alloys. The findings demonstrate that when the number of TBs increases, the yield strength of models with various numbers of TBs falls. The closer the location of TB to the upper surface of model, the lower the yield strength of the material. As the number of TBs increases, the obstruction of dislocation movement by TBs becomes more evident and the degree of plastic deformation of the surface of the model after bombardment becomes greater, making the material more susceptible to fracture. The closer the TB to the upper surface of the material, the more evident the inhibition of dislocation growth by the twin, which in turn affects the strength of the material. Deformation failure of the model is the combination result between dislocations and dislocations, dislocations and twins and other defects.

Key words: TiAl alloys; SFPB; twin boundary; molecular dynamics; mechanical properties

TiAl alloys are regarded as high-quality high-temperature light weight materials in modern aero-engines and automobiles because of superior properties such as low density, high specific strength, high specific stiffness and high temperature corrosion resistance[1–3], which is mainly used in turbine blades and compressors of aero-engines to reduce the weight of aero-engine parts and thus to reduce the overall weight of the aircraft[4–7]. However, with the improvement of process technology, some practical applications put forward higher performance requirements for TiAl alloys. Therefore, it is increasingly urgent to strengthen the surface of TiAl alloys and to improve their high-temperature performance[8].

Studies have found that most material components fail on the surface of the material, so improving the surface properties can have a positive effect on the overall performance of the material[9]. At present, research on the surface mechanical properties of titanium-aluminium alloys has been conducted in-depth. Feng et al[10] modeled the effect of roughness variation on the cutting process of γ-TiAl alloys, and the results showed that the greater the roughness, the more likely the defect occurrence. The effect of roughness on the removal mechanism of γ-TiAl alloys was further investigated by Yang et al[11]. It is found that the surface weave density increases with increasing roughness. Surface strengthening technology is an effective method to improve the surface properties of materials, and the commonly used surface strengthening methods mainly include: high-energy shot peening, supersonic fine particle bombardment (SFPB), surface mechanical grinding, laser pulse shot peening and ultrasonic impact[12–13]. SFPB[14], as one of the surface strengthening technologies with

Received date: May 29, 2023
Foundation item: National Natural Science Foundation of China (52065036); Key Program of Natural Science Foundation of Gansu (23JRRA760); Natural Science Foundation of Gansu (22JR5RA298); Hongliu First-Class Disciplines Development Program of Lanzhou University of Technology
Corresponding author: Feng Ruicheng, Ph. D., Professor, School of Mechanical and Electrical Engineering, Lanzhou University of Technology, Lanzhou 730050, P. R. China, Tel: 0086-931-5135199, E-mail: postfeng@lut.edu.cn

considerable development prospects in recent years, has strong application flexibility and high processing efficiency. This technology can be used for the nano-surfacing of complex shapes and large areas of metallic materials and is suitable for a large number of industrial applications, making up for the shortcomings of other previous surface nano-surfacing technologies. This provides a basis for the industrial application of surface nano-chemistry[15]. The surface strengthening of TiAl alloys has been indepth researched. Wu et al[16] studied the effect of performance changes of SFPB on the surface of lamellar TC11 titanium alloy after nano-treatment using gas pressure as a variable, and the results showed that the yield strength is improved to a certain extent. Zhang et al[17] experimentally tested the high circumferential fatigue properties of TC11 titanium alloy after surface strengthening by SFPB at different temperatures. It is found that the nano-sized surface of TC11 titanium alloy and the SFPB treatment cause the surface crack source to move down to the sub-surface layer of the alloy. Chen et al[18] analyzed the influence of different shot peening parameters on the gradient nanostructure TC4 titanium alloy using the pressure and time as variables of shot peening. The results show that the thicknesses of the gradient nanostructure and deformation layer formed after shot peening grow with the increase in shot peening parameters, and finally the thickness of the deformation layer tends to be stable, so the grain size and strengthening degree are gradually saturated. Cong et al[19] analyzed the mechanical properties of ultrasonically tumbled and polished 2D12 aluminium alloy, and the experimental results showed that the mechanical properties of the ultrasonically treated material are significantly improved.

Twin reflects parts of crystals and the symmetrical position relationship between crystals with respect to a common crystal[20]. Studies have shown that the introduction of twin boundaries (TBs) in nanomaterials is a novel way of strengthening[21–24]. A large number of scholars have studied the mechanical properties and deformation mechanism of nanotwin materials. An et al[25] used the molecular dynamics (MD) method to study the influence of twin spacing in Al crack propagation, and the results showed that there is an optimal mechanical property near the critical twin spacing. Forwood et al[26] found that the number of TBs is related to the strong plasticity of TiAl alloys, and the increase in the number of twins has a positive effect on the improvement of strong plasticity. Cao et al[27–28] believed that different TB spacings affect dislocation behavior. The crack deformation mechanism of twin γ-TiAl alloys is TB migration, twin formation, and the interaction between cracks and twins[29]. And TBs are helpful to improve the strength of γ-TiAl alloys. Through MD simulations, Wang et al[30] demonstrated that the yield strength of nano-twinned titanium exhibits an initial increase followed by a decrease with the reduction in twin density at ambient temperature, suggesting the presence of a critical twin density threshold in this material.

Scholars have fully studied the performance and microstructure evolution of TiAl alloys in SFPB experiments[31]. For the study on the mechanical properties and deformation mechanism of TiAl alloys under SFPB treatment, it is necessary to explore the deformation mechanism from the atomic scale and should be combined with existing experimental reports. In this research, SFPB simulations were conducted on TiAl alloys at different TB locations and with different quantities from the atomic scale to compare and to analyze the changes in mechanical properties and microstructural evolution of TiAl alloys after bombardment.

1 Models and Methods

1.1 Simulation model

For studying the influence of the number of TBs on the mechanical properties and microstructure evolution of TiAl alloys after SFPB, four bombardment models containing different TB numbers were established. And the TBs gradually increased from 1 to 4. The TBs in all models were evenly distributed in the matrix[24,26,32]. The overall dimensions were the same for all four models, with lengths of L_a=21.3 nm in the x-direction, L_b=19.2 nm in the y-direction and L_c=33.2 nm in the z-direction. And the total number of atoms in the model is 842 400. The single crystal of TiAl alloys was a face-centered tetragonal (fct) structure, with lattice parameters a=b =0.4001 nm, c=0.4181 nm, and axial ratio c/a=1.04. The grain orientations of the adjacent two layers in the matrix model were $[\bar{1}10]$, $[\bar{1}\bar{1}2]$, [111] and $[1\bar{1}0]$, $[\bar{1}\bar{1}2]$, $[\bar{1}\bar{1}\bar{1}]$. Fig. 1a reveals 4-twin boundaries matrix model. Fig. 1b shows a model of SFPB with four TBs. Fig. 1c shows the MD model. The main parameters of the SFPB simulation are shown in Table 1.

To study the effects of different twin positions on the deformation mechanism and tensile mechanical properties of TiAl alloys after SFPB, atomic models with different TB positions were established. After the MD simulation of atomic impact models with different TB positions in the early stage, the data were analyzed and compared. Finally, three groups of different TB positions were selected to establish the model, and the positions were 1/2, 1/3 and 1/5 from the upper surface of the matrix[33]. Taking the TB at the 1/2 position as an example, Fig. 2 shows a model of the atoms with the TB located at the 1/2 position on the surface of the substrate and a schematic diagram of the locally enlarged atoms. In this model, the overall size, the total number of atoms, and the crystallographic orientation of the two adjacent layers of atomic grains in each axis remain the same as those in the model in Fig. 1. The parameters of the SFPB simulation remain consistent with those in Table 1.

1.2 Simulation methods

MD simulations were performed by LAMMPS[34] software. The atomic interaction potential was used to describe interatomic interactions, and the choice of the potential function was particularly important to make the simulation results more accurate. Using a modified EAM[35] potential, the mechanical relationship between this individual model and the whole was described through a functional expression by

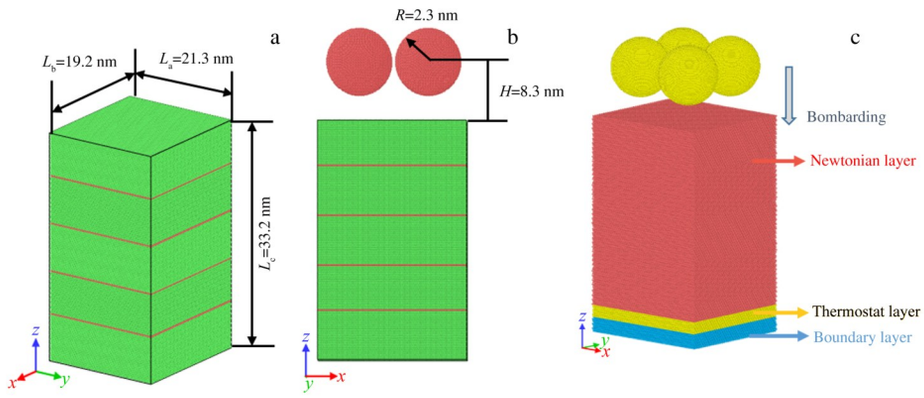

Fig.1 SFPB model: (a) 4-twin boundaries matrix model, (b) 4-twin boundaries bombardment model, and (c) MD model

Table 1 Main simulation parameters of SFPB

Parameter	Value
Radius of pellets/nm	2.3
Number of pellets	4
Pellet speed/m·s^{-1}	3800

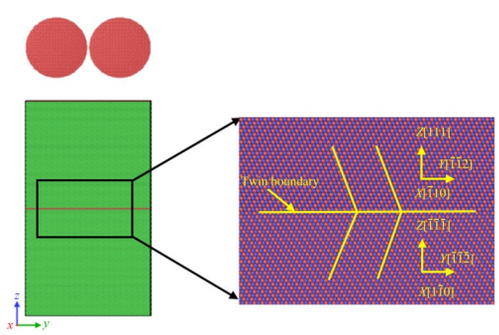

Fig.2 Local enlargement of the model with the TB located at 1/2 of the upper surface of the substrate

studying each atom in the collective, and the sum of the mosaic energy and the interaction potential energy was the total energy of the system. This potential function has been applied in the simulation of TiAl alloys[36–37].

The basic equation of the potential energy function is as follows:

$$U = \sum_{i}^{N-1} \sum_{j=i+1}^{N} \varphi\left(r_{ij}\right) + \sum_{i=1}^{N} F\left(\rho_i\right) \quad (1)$$

where U represents the total potential energy of the system, N is the total number of atoms, the subscripts i and j represent the number of atoms in the system, r_{ij} refers to the distance between atom i and atom j, $\varphi\left(r_{ij}\right)$ describes the pair potential, and $F\left(\rho_i\right)$ represents the embedding energy.

$$\rho_i = \sum \psi\left(r_{ij}\right) \quad (2)$$

where $\psi\left(r_{ij}\right)$ is the density function[30].

This study is bifurcated into two parts. Firstly, the SFPB process was simulated. Secondly, the tensile properties of the model were investigated after the bombardment. In the bombardment process, the velocity set method was used to set the atomic velocity of the bombardment along the z-direction. Free boundary conditions were applied in the z-direction, while periodic boundary conditions were employed in other directions, and the system was maintained at a temperature of 300 K. First of all, relaxation in the NVE ensemble was set, and the relaxation time was 50 ps. After completion of relaxation, bombardment simulations were carried out in the NVT ensemble with three bombardments of 14 ps each. With deform stretching, the z-direction was a free boundary condition, and the rest of the directions were periodic boundary conditions. The first relaxation was 100 ps in the NPT ensemble, followed by stretching in the NVT ensemble. The atomic position, temperature and energy were output every 1000 steps. Post-processing analysis was performed by OVITO[38] software. The common neighbor analysis (CNA)[39] was used to analyze changes in defects such as layer dislocations and vacancies due to atomic structure deformation. In addition, the dislocation extraction algorithm (DXA)[40] was employed to analyze changes related to characterized atomic dislocations.

2 Results and Discussion

2.1 Effect of number of TBs on tensile mechanical properties

The influence of TB number on the tensile mechanical properties of TiAl alloys after SFPB is studied by changing the number of TBs. Fig. 3a shows the stress-strain curves obtained for models with different numbers of TBs for a bombarded model subjected to tension in z-direction. Fig. 3a reveals that the number of TBs has a large influence on the tensile mechanical properties of the material[26,32]. The stress-strain curves are mainly divided into two stages: elastic deformation and plastic deformation. In the elastic deformation stage, the stress of each model increases with the growth of strain, showing a linear change, followed by a rapid decrease in stress. When the strain is around 5%, there is a small change in the stress-strain curve for each model. The stress at the peak of the curve is the yield stress, and the strain

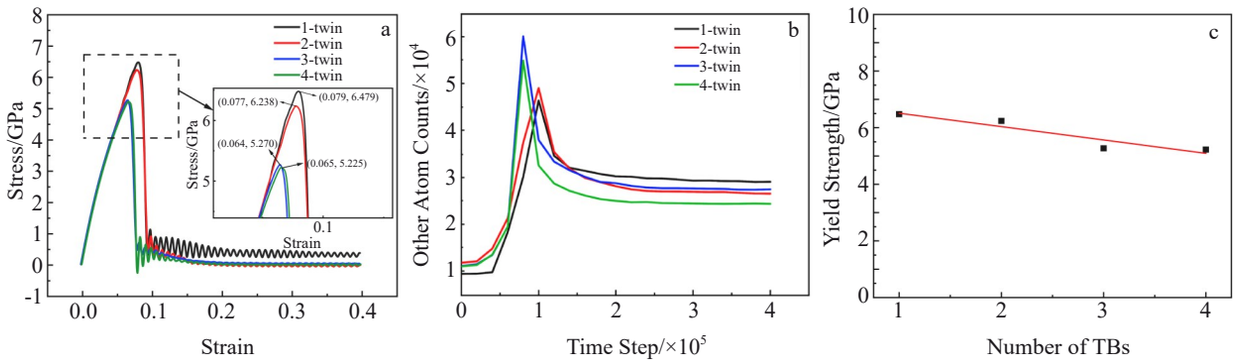

Fig.3 Stress-strain curves (a), other atom counts versus time curves (b), and yield strength as a function of TB number (c) for models with different twin numbers

corresponding to the yield strength varies from model to model in the diagram. The 1-twin model has a maximum yield strength of 6.47 GPa and a failure strain of 7.92%, which is greater than those of the 4-twin model with a yield stress of 5.22 GPa and a failure strain of 6.56%. In the elastic deformation stage, the stress increases and accumulates under the action of strain and produces a large number of defects such as dislocations. When the stress reaches the critical stress, the dislocation slip system is activated and emits dislocations, thus releasing the accumulated stress and energy and eventually causing the material to fracture and fail. Unlike the results of most studies, the yield stress in this study shows a decreasing trend with increasing the number of twins. That is to say, it increases with the growth of the twin spacing[41]. One of the reasons for this phenomenon is the presence of defects, such as small voids and vacancies, on the surface of the material after SFPB. The tensile mechanical properties of the material with defects after surface treatment may not be the same as that of most pre-twinned materials without surface treatment. This conclusion is consistent with the conclusion of Cao[28–29], i. e., "the peak stresses of cracked models with different twin spacing were significantly smaller than those of uncracked models". At the same time, because of the presence of TBs, the dislocations are limited to slip within the single crystal and no longer grow. This phenomenon becomes more pronounced as the number of TBs increases. In the model containing 1 TB, the twin is located in the middle and the dislocations can grow in a large area. After relaxation of the bombarded model, an energy balance is achieved in the system. Dislocations become entangled with each other, resulting in dislocation pinning phenomenon. There may be a large number of pressure stair-rod dislocations that exist to form stacking fault tetrahedra (SFT), which contributes to the maximum yield strength of the 1-twin model. The SFT is a three-dimensional vacancy defect consisting of four {111} faces and six differently oriented stair-rod dislocations. It is produced at high speeds with large deformations. During SFPB, a large number of vacancies gather and form vacancy clusters, and a large number of Shockley dislocations meet by slip and merge to become stair-rod dislocations. As the bombardment progresses, the SFT structure breaks down, requiring a large amount of energy to do so. A large number of dislocations are created as the SFT breaks down. This leads to an increase in the yield strength of the material.

This result is in agreement with the results of Xue et al[42] who studied the effect of twinning distance on the properties of tungsten nanoparticles.

A large number of disordered atoms are generated during plastic deformation of the material, and the weak interaction force between disordered atoms makes the material more prone to deformation failure, so the change in the number of disordered atoms affects the yield strength of the material. Fig.3b shows the graph of the number of disordered atoms as a function of time during stretching for models with different numbers of TBs. Combining Fig.3a and 3b, it is observed that the 1-twin model has the lowest number of disordered atoms at the peak stress. In contrast, the model containing 4 TBs has the highest number of disordered atoms, and a large number of disordered atoms are generated when dislocations and interfaces interact. This negatively affects the tensile mechanical properties of the material and thus reduces the yield stress of the TiAl alloys[43]. It is observed from the Fig.3c that the yield stress tends to decrease with the increase in the number of twins. The yield strength of the model with 4 TBs is decreased by 19.3%, compared with that with 1 TB, indicating that the number of TBs has an effect on the yield strength of the material, and it basically satisfies the linear relationship, as shown in Eq.(3).

$$\sigma = 6.98 - 0.47X \quad (3)$$

where X denotes the number of twins and σ denotes the yield strength.

A comparison of the tensile stress-strain curves for the models with different numbers of TBs shows that the peak strength required for fracture failure varies with the number of TBs in models. The strain at yield strength also varies between the models, and the difference between the 1-twin and 2-twin models is small, but the yield stress for the other two models is much smaller than that of the 1-twin and 2-twin models. This phenomenon is the result of the evolution of microscopic defects during tensile deformation in each model. In combination with the above conclusions, the yield strength of the material varies with the number of TBs. As the number

of TBs increases, the yield strength of the material decreases.

2.2 Influence of number of TBS on tension and bombardment deformation mechanism

By studying the relationship between mechanical properties of TiAl alloys models and TB quantities, it is found that the number of TBs affects the tensile mechanical properties of models. In order to further investigate the stress response, it is necessary to analyze the evolution of the microstructure to reveal the effect of the number of TBs on the tensile deformation mechanism of TiAl alloys by SFPB. It has been shown that there are three main tensile deformation mechanisms of dislocation-twin reaction and Shockley partial dislocation slip, which are dislocation piling up and crossing TBs, Shockley partial dislocation inducing TB migration, and restricting slip of penetrating dislocations within twin layers[44–45]. Fig.4 shows the evolution of the microstructure of a TiAl alloys with 1-twin model under tensile loading. For 1-twin TiAl alloy model with large TB spacing, twin migration and incomplete dislocation are the main tensile deformation mechanisms. The bombardment-treated model in Fig.4a has defects such as stacking faults and vacancies at TB and a small number of bcc atoms exist when the load is applied at the beginning. When the tensile strain increases to 5.69%, a large number of dislocations are emitted inside the crystal and accumulated at the TBs. Because of the high grain boundary storage energy in the TBs, when the tensile load on the model becomes large, the energy at the TBs is higher and the movement of atoms here is relatively easy, resulting in the generation of defects such as vacancies and interstitial atoms. Dislocations react with each other to produce dislocation tangles and dislocation loops, while reactions between partial dislocations on two intersecting dislocation slip surfaces can be seen to form a stair-rod dislocation, and the Lomer-Cottrell lock is shown in Fig.4b[46]. In Fig.4c and 4d, the number of bcc atoms and disordered atoms increases with increasing tensile load, producing numerous stacking faults. At this point, there is a larger stress and energy in the interface. When the number of dislocations at the twinning boundary reaches a certain level, it causes bending deformation at the twinning interface, leading to material detwinning. When the stress and energy at the twin interface accumulate to saturation values, the interface starts to become unstable. Then, the stress and energy are released, causing the TB to act as a source of dislocation emission to the surrounding area, which allows the system to stabilize. Point defects such as high-density vacancies and interstitial atoms at the interface successively trigger the generation of tiny holes, which continuously expand into cracks, and cracks eventually lead to model fracture. The model fracture is the result of the combined action of dislocation motion, phase transformation and crack extension, as shown in Fig.4f. The phenomenon of secondary twin generation and migration is also found during the deformation process, and dislocations moving parallel to the TB are also observed in Fig.4e and 4f, which are not observed during the tensile deformation of other models with twins.

Fig.4g–4i are DXA analysis plots corresponding to Fig.4b–4d, respectively. It is observed that dislocations and TBs interact with each other to deform the TiAl alloys, where the main types of dislocations are Shockley partial dislocation and stair-rod dislocation, followed by a small number of other types of dislocations. Through comparison and analysis of the DXA diagrams of four models with different numbers of TBs, it can be observed that the number of stair-rod dislocations during continuous tensile deformation in the 1-twin TiAl alloys model is significantly higher than that of the remaining three models. This phenomenon may partially account for why the yield strength of the 1-twin model is greater than that of the other three models.

Fig. 5 shows the microstructural evolution of the 2-twin TiAl alloys in deforming and failing under different tensile loadings. Fig. 5e–5g are the DXA diagrams corresponding to Fig. 5a – 5c, respectively. Compared with the wide-spacing grain boundaries of 1-twin model, the dislocation reaction space becomes relatively smaller during the stretching of the 2-twin model. Analysis of Fig. 5 shows that dislocation slip, stacking fault generation, and dislocation-twin interface reactions are closely related to the deformation failure of TiAl alloys. The types of dislocations during tensile deformation are mainly Shockley partial dislocation and stair-rod dislocation, where the number of stair-rod dislocations is less compared with that in Fig. 4, and the stair-rod dislocation, as an immobile dislocation, acts as an obstruction to the dislocation movement, and this obstruction effect has a positive effect on the TiAl alloys. The reduction of the stair-

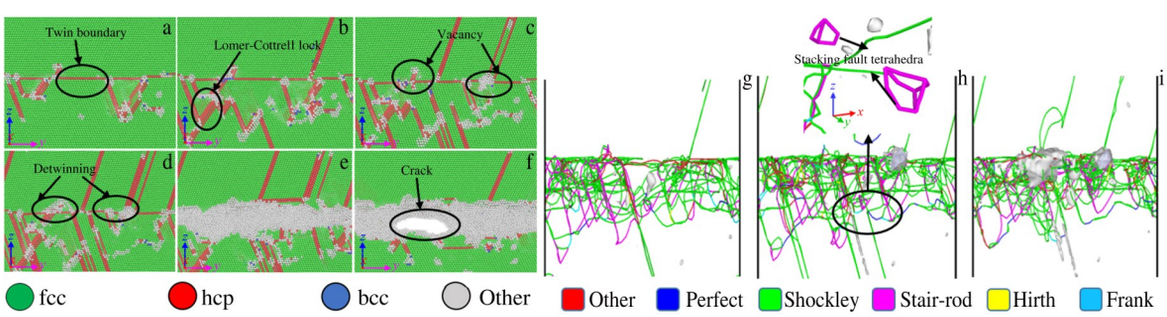

Fig.4 CNA (a–d) and corresponding DXA plots (g–i) of 1-twin model under different tensile loads: (a) ε=1.75%, (b, g) ε=5.69%, (c, h) ε=6.74%, (d, i) ε=7.89%, (e) ε=8.75%, and (f) ε=9.03%

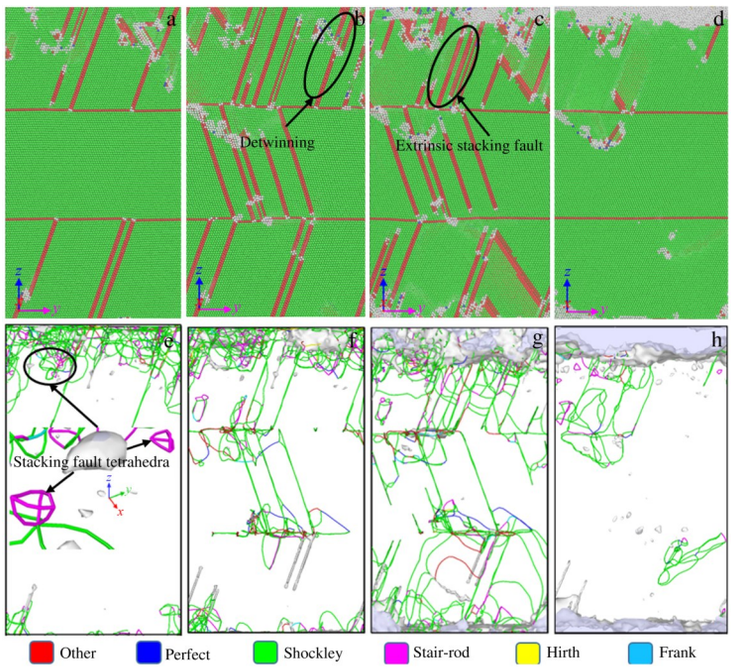

Fig.5 CNA (a–d) and DXA (e–h) plots of the 2-twin boundaries model under different tensile loads: (a, e) ε=2.80%, (b, f) ε=6.85%, (c, g) ε=7.80%, and (d, h) ε=8.79%

rod dislocation is one of the reasons why that of the 2-twin model is less than that of the 1-twin model. During the tensile deformation process of the 2-twin model, there are also dislocation-dislocation reactions, interactions between dislocations and TBs, and dislocation tangling on the surface. It is observed that the number of dislocation tangles is less than that of the previous model. In addition, only a small number of bcc atoms are present in the atomic configuration diagram of Fig.5.

When the strain is 2.80% as shown in Fig.5a, the Shockley partial dislocation on the surface emits dislocations toward TB, and after reaching the interface, the dislocations accumulate at the grain boundary due to the blocking effect of the TB and the relatively little mutual reaction between the dislocations. When the strain increases as shown in Fig.5b–5c, after the accumulated dislocations reach a certain number, a large amount of energy and stress concentration exist at the interface, making the system unstable. At this point, the TB as a dislocation source releases the dislocation moving towards the surface or another twin, allowing the system to stabilize again, during which plenty of disordered atoms are generated. Surface bombardment treatment can lead to the formation of many defects, such as dislocations and vacancies. During the tensile deformation process, the originally disordered atoms on the surface become tiny voids under continuous strain, and then they develop into cracks that are propagated through the material until the alloy ultimately fractures. In this process, the dislocations at the TBs react with the twin interface to cause a certain degree of damage to the interface, but due to the obstruction of dislocations by the twins, the failure process at the TBs is slower than the fracture failure process at the surface of the substrate. Finally, the TiAl alloy model containing 2 TBs fractures and fails on the surface, as shown in Fig.5d.

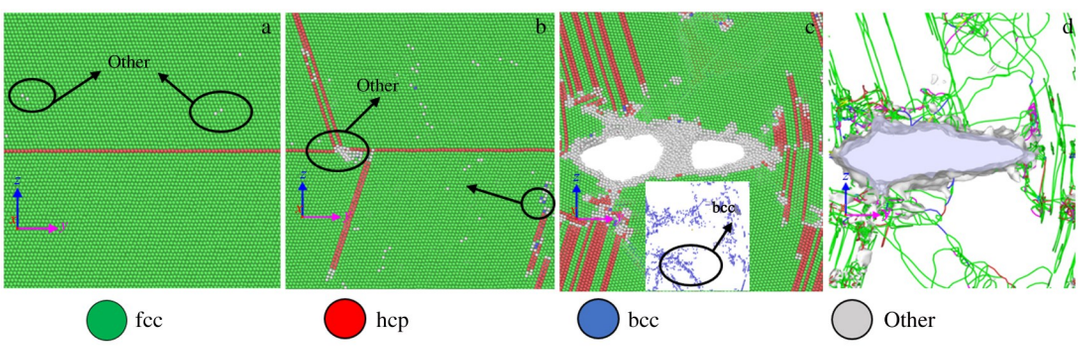

Fig.6 CNA (a–c) and DXA (d) diagrams during deformation failure of 1-twin boundary model without SFPB: (a) ε=11.2%, (b) ε=12.2%, and (c, d) ε=13.2%

For investigating the effect of SFPB treatment on the properties of TiAl alloys, the microstructure of 1-twin TiAl alloy model is compared and analyzed under different tensile loads after bombardment and non-bombardment treatments, as shown in Fig.4 and Fig.6, respectively. Fig.6a–6c show CNA diagrams of unbombarded models under different tensile loads, with a small number of bcc atoms and other atoms produced in the pre-plastic deformation period. In Fig.4f and Fig.6c, both models fail by fracture at the TB, but the tensile deformation mechanism of the unbombarded model is dominated by the phase change, as shown in the small diagram in the lower right corner of Fig.6c. The dislocations are mainly Shockley incomplete dislocations and a few stair-rod dislocations, without SFT production, as shown in Fig.6d. The bombardment-treated models produce a small number of SFTs, in addition to the Lomer-Cottrell lock structure, which has a positive effect on the material strength enhancement.

In order to investigate the microstructure evolution of models with different TB numbers under bombardment, CNA analysis was conducted for each model. The results indicate that compared with the other two bombardment processes, the plastic deformation degree of each model is the highest after the first bombardment, and the degree of surface plastic deformation is closely related to dislocation changes. Therefore, the OVITO software was used to extract and to analyze the total number and length of dislocations following the initial bombardment in each model. It is observed that there are peaks in both parameters after the first event. Fig.7 shows the total number and total length of TiAl alloys with different numbers of TBs at the peak point of dislocation after the first bombardment. It can be seen that the total number of dislocations in samples with 1-twin, 2-twin, and 3-twin models decrease gradually, and the total value of dislocations in 4-twin model is greater than that in 3-twin model. After the first bombardment, the total length of each model reaches the peak value, and the peak value of the total length of the dislocation is in the order from the highest to the lowest of 4-twin, 1-twin, 3-twin, and 2-twin.

By analyzing the total number and total length of TB

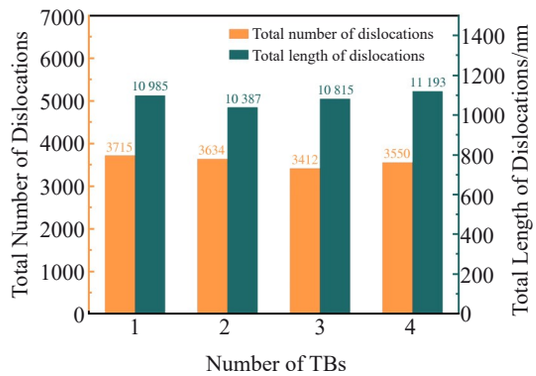

Fig.7 Histogram of total dislocation length and total number of dislocations at the peak dislocation point after the first bombardment for different models

models with various dislocations following initial bombardment, it is evident that alterations in dislocation impact the plastic deformation mechanism of each model during the bombardment. In order to investigate the deformation mechanism of each model throughout the entire bombardment process, we characterized the microstructure of models with different TB numbers at the same moment after completion of bombardment, as illustrated in Fig.8a–8d. The microstructural analysis of each model by CNA and DXA techniques reveals that the plastic deformation mechanism in 1-twin model is primarily driven by the interaction between a significant number of Shockley dislocations and other types of dislocations. The mechanism of the remaining three models involves dislocation-twin and dislocation-dislocation reactions. The dislocations of these three models are impeded by the TB upon bombardment, resulting in their accumulation and entanglement at the interface due to its obstructive effect. This phenomenon ultimately leads to a higher degree of surface plastic deformation for the other three models compared with that of the 1-twin model, as depicted in Fig.8b–8d.

The above study shows that the degree of bombardment plastic deformation of models with different numbers of TBs

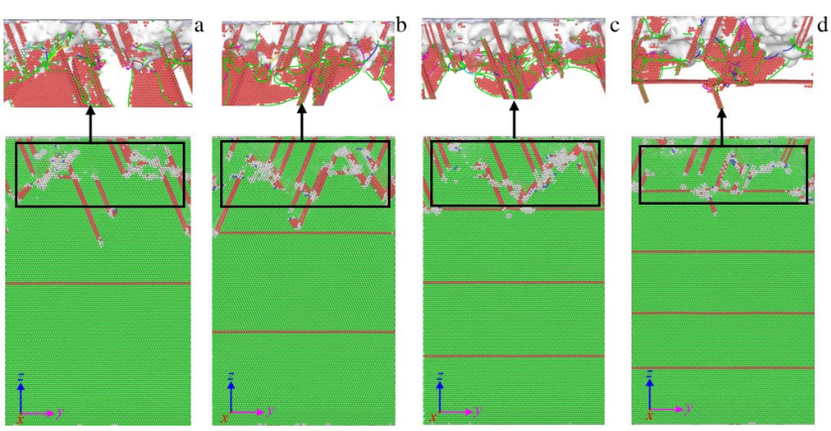

Fig.8 CNA and DXA plots at the same moment after bombardment for different models: (a) 1-twin model, (b) 2-twin model, (c) 3-twin model, and (d) 4-twin model

after SFPB varies. The presence of TBs can impede the movement of dislocations, resulting in a higher degree of bombardment plastic deformation for materials with smaller number of TBs. These TBs have an impact on the tensile properties of the material and may contribute to the material's propensity to fracture during tensile deformation. By comparing the differences that exist during tensile deformation in each model, it is found that the 1-twin model fractures and fails at the TB, while fracture in the other three models occurs on the surface. Starting from the microstructure of each model, dislocation slip and dislocation-twin are the main response mechanisms in the 1-twin model, and mechanisms of the other models are vacancy defect evolution accompanied by a small amount of dislocation slip and some dislocation-twin reactions. Also, the number of dislocations in the compression bar in the 1-twin model is greater than in the other models. These differences ultimately result in the 1-twin model having the highest yield strength, with the rest of the models decreasing in order. It is also found that the models relax at the end of bombardment, and SFT is generated, which can be observed in Fig.4, Fig.5, and Fig.10. The reason is that relaxation is the process of stabilization of the matrix energy, and a large number of Shockley dislocations merge into stair-rod dislocations, and stair-rod dislocations generate SFTs. It has been shown that the size of SFT affects the strength of single-crystal materials[47], and the number of SFTS in the 1-twin model is predominant in this study, and as the tensile load increases, the size of the tetrahedra slowly increases and finally the stair-rod dislocation starts, prompting its decomposition.

2.3 Effect of TB position on the tensile mechanical properties

The effect of TB location on the tensile mechanical properties of TiAl alloys after SFPB was investigated by varying the TB location (1/2, 1/3 and 1/5 of the upper surface of the substrate). From the stress-strain curves in Fig. 9a, different locations of TBs lead to variations in the yield strength of the three models. The model with the TB located at 1/2 of the upper surface of the substrate exhibits the highest yield stress value of 6.47 GPa, while the model with the TB positioned at 1/5 of the upper surface of the substrate has the smallest yield strength, 4.91 GPa. The variations in the yield strength of the models with TBs at three different locations indicate that the location of the TB affects the tensile mechanical properties of the TiAl alloys, while the effect of the location of the TB on the elastic modulus is not significant, as shown by the slope of each curve [48]. When the yield stress is reached, the model with the TB located at 1/2 from the upper surface of the substrate shows a greater strain compared with that of the other two models with different twin positions. During the elastic deformation phase, the curves follow approximately the same trend, and stress gradually linearly rises as tensile strain increases. Because of the nucleation of Shockley incomplete dislocations on the surface of the matrix and at the twin interface during tensile deformation, the number of dislocations increases at a rapid rate due to the continuous emission of dislocations. At the same time, due to the presence of twin, a large number of dislocations accumulate and nucleate at the twin faces, and the accumulated dislocations eventually cause the material to undergo strain hardening [29].

When the stress reaches a range which the interface cannot withstand, the dislocation-twin and the twin interface act as a dislocation source emitting dislocations, thus causing the stress to drop rapidly and releasing energy. Fig. 9b shows a plot of the total length of dislocations versus strain for TiAl alloy models at different TB positions. The trend is similar to the stress-strain diagram, a rise followed by a sharp fall and a final stabilization. The rising phase of the total dislocation length corresponds to the strain-hardening phase of the stress-strain curve, and its rapid falling phase is the deformation failure phase of the TiAl alloys in the stress-strain curve. The total length of dislocations is reduced due to the disappearance of some dislocations as a result of defects such as holes and cracks created during the fracture failure of the material. The total length of each dislocation is the maximum at its corresponding yield strain, and the strain corresponding to the maximum total length of the dislocation is consistent with the strain corresponding to the yield strength in the stress-strain curve.

By comparing the tensile stress-strain curves for the models with different TB locations, it is found that the peak strength required for fracture failure differs between the models, depending on the location. Also, as observed from the curves, there are differences in the strains required to reach yield

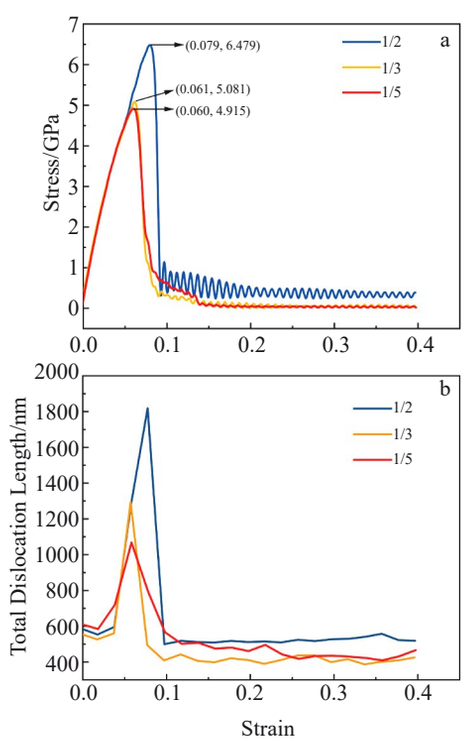

Fig.9 Stress-strain curves (a) and total dislocation length (b) for different twin location models

strength for each model, meaning that the higher the strain required for the material to fracture and to fail, the less likely it is to be destroyed and at the same time the higher the yield strength. This is mainly due to different deformation mechanisms of the material during tensile failure. In summary, the yield strength of the material varies, depending on the location of the TB. As the TB gets closer to the upper surface of the substrate, the yield strength decreases. This phenomenon is the result of the combined effect of dislocations-dislocations, dislocations-twin as well as the defects.

2.4 Influence of TB position on tension and bombardment deformation mechanism

By studying the tensile mechanical properties of TiAl alloy models at different TB locations (1/2, 1/3 and 1/5 of the upper surface of the substrate), it is found that to further investigate the tensile mechanical response, it is necessary to analyze the microstructure evolution to reveal the effect of TB location on the tension and bombardment deformation mechanism of TiAl alloys by SFPB. The atomic evolution diagrams of the models with TBs positioned at 1/2 from the upper surface (including 1-twin boundary) in tensile failure are described in Section 2.2. Fig. 10 and Fig. 11 show the evolution of the tensile deformation failure of the model with the TB located at 1/3 and 1/5 from the upper surface of the substrate, respectively. In Fig.10a, at a strain of 4.70%, a small number of disordered atoms are present on the surface of the substrate. A large number of Shockley partial dislocations and stair-rod dislocations, as well as a few other dislocations dominate the deformation process. As strain increases, disordered atoms on surface increase and defects such as stacking faults, secondary twins, and Lomer-Cottrell locks arise and evolve, as shown in Fig. 10b – 10c. At the same time, Fig. 10d shows that the secondary twins constantly migrate under the dominance of Shockley partial dislocation, and finally the surface evolves from the initial disordered atoms to the vacancies and to the holes and cracks under the increasing tensile strain[29]. Fig.10e–10h are the DXA plots corresponding to Fig. 10a – 10d, respectively. The material fracture failure causes most of the dislocations to annihilate and the number of each type of dislocation drops sharply in Fig.10e–10h.

The microstructural deformation of the model is related to the dislocation reaction. Fig.11e shows the DXA diagram at a strain of 7.80%, and an extended dislocation reaction expression is observed by analysis.

$$1/2\left[\bar{1}01\right] = 1/6\left[\bar{1}12\right] + \mathrm{SF} + 1/6\left[\bar{2}\bar{1}1\right] \quad (4)$$

where $1/2\left[\bar{1}01\right]$ is an extended dislocation with bundle set, SF is stacking fault sandwiched between two incomplete dislocations. The larger the width of SF, the smaller the stacking fault energy per unit area. After the two partial dislocations are partially obstructed, the width of the stacking fault becomes smaller, and finally it shrinks to perfect dislocations, i. e., bundle sets are formed. After this perfect dislocation appears under the action of external forces, it decomposes into partial dislocations for slip.

The tensile deformation process of the model with twin located at 1/5 from the upper surface of substrate is shown in Fig. 11a–11d. Comparing the CNA diagrams of Fig. 10b–10c

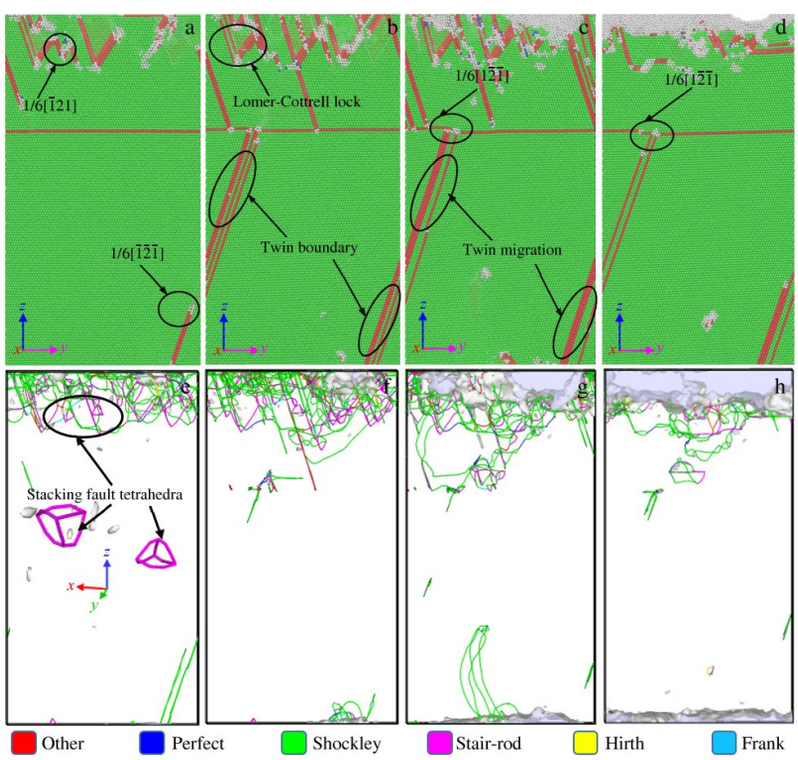

Fig.10 CNA (a–d) and DXA (e–h) diagrams of the tensile failure process of a model with TBs located at 1/3 of the upper surface of the substrate: (a, e) ε=4.70%, (b, f) ε=5.69%, (c, g) ε=6.74%, and (d, h) ε=7.69%

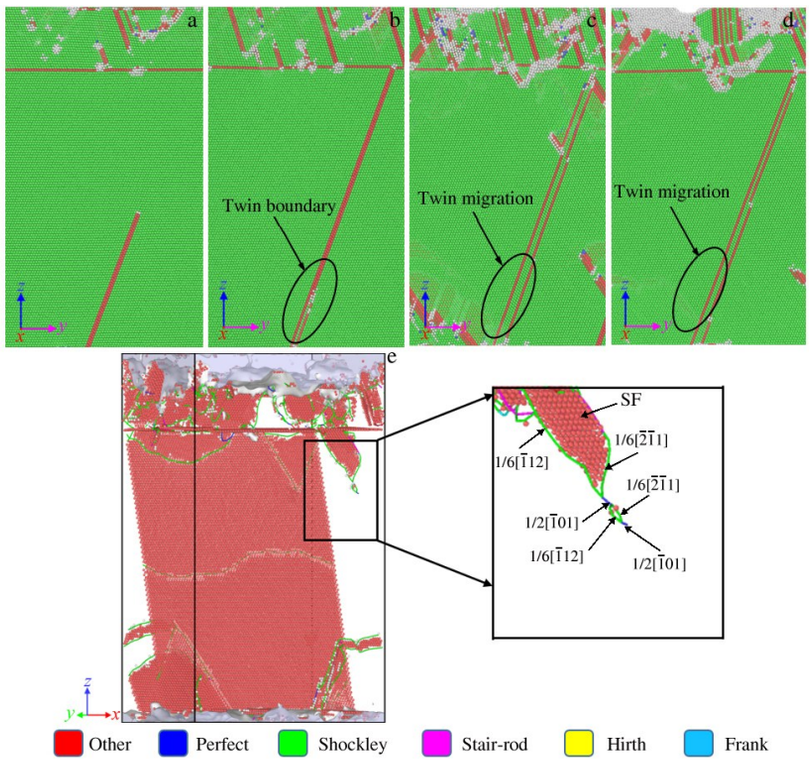

Fig.11 CNA (a–d) and DXA (e) diagrams of the tensile failure process of model with the TB located at 1/5 of the upper surface of the substrate: (a) ε=2.81%, (b) ε=5.82%, (c) ε=6.77%, and (d, e) ε=7.80%

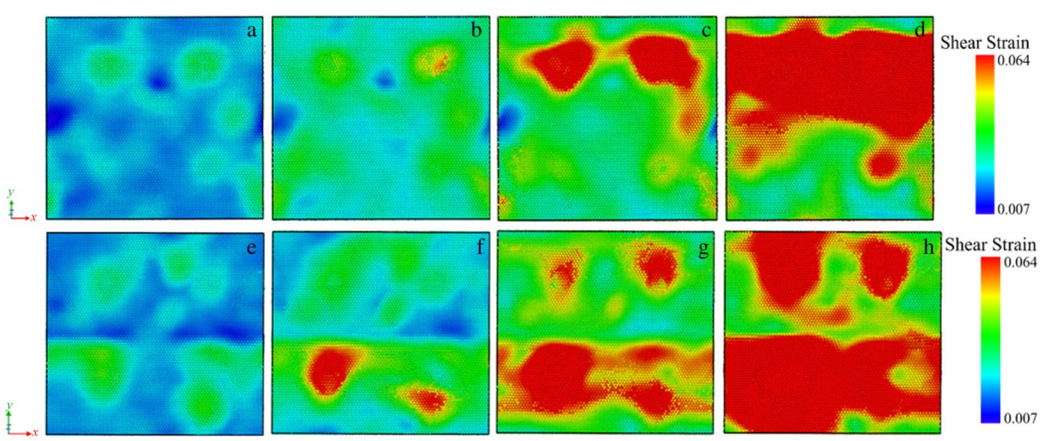

Fig.12 Shear strain distributions during tensile failure of models with TB located at 1/3 (a–d) and 1/5 (e–h) from the upper surface of the substrate

with Fig.11b–11c for the tensile deformation failure process, it is concluded that the number of defects such as stacking faults and secondary twins occurring in the tensile process in Fig.11 is less than that in Fig. 10. Meanwhile, it has been observed that the 1/3 position model exhibits a greater yield strain of roughly 6.14%, while the 1/5 position model has a lower yield strain of around 6.01%.

Fig. 12 shows the shear strain distributions during tensile deformation failure of model with the TB located at 1/3 and 1/5 from the upper surface of the substrate. From Fig. 12a–12d, it can be seen that the shear strain in the model of TB at the 1/3 position is mainly concentrated at the top two particles during the tensile process. As the tensile load increases, the model is firstly deformed at the position where the shear strain is greater, and eventually fails by damaging at the position where the deformation is the greatest, as shown in Fig. 12c–12d. Fig. 12e – 12h represent the shear strain distributions during tensile failure with the TB located at 1/5 of the upper surface of the substrate. Unlike the previous model, this model fails by fracture at the following two particle positions, as shown in Fig.12g–12h. Combining the stress-strain curves and microstructure diagrams of the two models, it can be observed

that the failure strain of the model with TB at 1/5 position is less than the model with TB at 1/3 position, and the strength of the model with TB at 1/3 from the upper surface of the substrate is higher than that of the model with TB at 1/5 position.

By comparing the differences in tensile deformation between the models, it is found that 1-twin model fractures and fails at the TB. In the other two models, fracture occurs at the surface with vacancy defect evolution, accompanied by a small amount of dislocation slip and some dislocation-twin reactions. The 1/3 model has significantly more defects such as dislocations and vacancies than the 1/5 model does. This is due to the difference in the distance between the upper surface and the TB in the two models. The shear strain during tensile failure shows that there is also a difference in the strains where the two models deform, and the 1/3 model shows a greater degree of plastic deformation than the 1/5 model at the same strain does.

Combined with previous studies on the tensile mechanical properties and deformation mechanisms of models subjected to SFPB, this study reveals the effects of TB positions on properties and mechanisms. The TiAl alloy surface is subjected to SFPB as a surface treatment. Therefore, it is imperative to conduct further investigations on the plastic deformation mechanism of each model under SFPB. To investigate the microstructure evolution of models with various TB positions under bombardment, CNA and DXA analyses are conducted on each model during the process. The results indicate that the plastic deformation mechanism of each model is affected by dislocation changes. Therefore, the total number and length of dislocations are extracted and analyzed after the first bombardment of models with different TB positions, as shown in Fig.13. After conducting CNA and DXA analyses, it is observed that the total number of dislocations and their overall length are peaked after the first bombardment. Furthermore, an increase in distance between the TB and upper surface of the matrix results in a corresponding increase in total length of dislocations. Fig.14

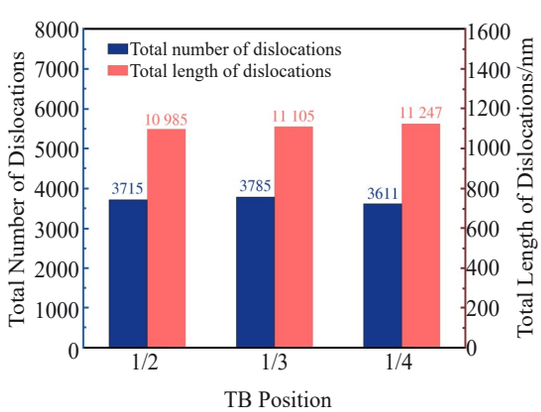

Fig.13 Histogram of total dislocation length and total number of dislocations at the peak dislocation point after the first bombardment for different TB location models

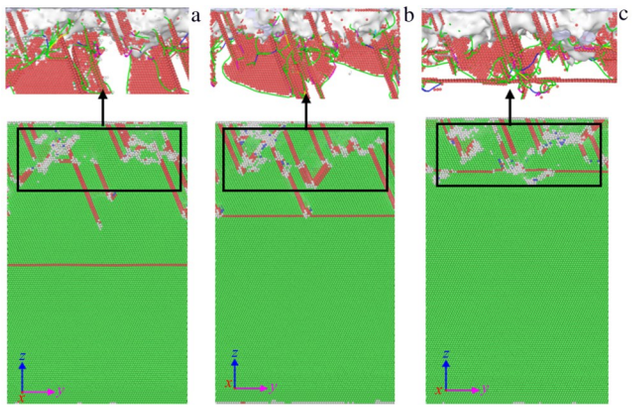

Fig.14 CNA and DXA plots of model with TB located at 1/2 (a), 1/3 (b), and 1/5 (c) from the upper surface of the substrate at the same moment after bombardment

depicts microstructure characterization for various models with different TB positions with equivalent time intervals of post-bombardment. The analysis of Fig.14 indicates that the degree of plastic deformation in the post-bombardment model varies with the position changes of the TB, and increases as it approaches closer to the upper surface, resulting in differences in tensile mechanical properties among these models.

3 Conclusions

1) There are differences in yield strength between models with different numbers of twin boundaries (TBs) treated with supersonic fine particle bombardment. The yield strength decreases as the number of TBs increases. The 1-twin model has the highest yield strength. The stacking fault tetrahedra generated during the tensile process increases the yield strength of the material.

2) The tensile deformation mechanism differs between the models with different TB numbers. The 1-twin bombardment model has dislocation-twin interactions and TB migration as the tensile deformation mechanisms, whereas the unbombarded model is dominated by phase transformation. The remaining three models are characterized by a combination of surface vacancy evolution, dislocation slip and the combined effect of dislocation-twinning.

3) The yield strength of the model at different TB locations after SFPB varies, and the yield strength decreases as the distance between the TB and the upper surface of the substrate decreases. The highest yield strengths are found for model with the TB located at 1/2 from the upper surface of the substrate.

4) The tensile deformation mechanism for each TB location model is a result of the combination of dislocation-dislocation, dislocation-twin and vacancies. The tensile failure of 1/3 and 1/5 models is mainly due to the evolution of defects such as vacancies. Both the number and location models of TB of bombardment plastic deformation mechanisms are dominated by dislocation slip and dislocation-twin reaction.

References

1 Qin R Y, Zhang G Y, Li N *et al. Journal of Mechanical Engineering*[J], 2021, 57: 115

2 Wang J, Cao T W, Chen C *et al. Aerospace Manufacturing Technology*[J], 2022, 65: 14

3 Wang M S, Du Y L. *Journal of Aeronautics*[J], 2021, 42: 8

4 Loria E A. *Intermetallics*[J], 2001, 12: 997

5 Nochovnaya N A, Panin P V, Kochetkov A S *et al. Metal Science and Heat Treatment*[J], 2014, 56: 364

6 Ye X C, Xiao K Q, Cao R X *et al. Vacuum*[J], 2019, 163: 186

7 Chen C Y, Wang J, Wang R X *et al. Science & Technology Review*[J], 2023, 41: 34

8 Dong M L, Jin G, Wang C H *et al. Nonferrous Metal Engineering*[J], 2021, 11: 22

9 Zheng H Z, Guo S H, Luo Q H *et al. Journal of Iron and Steel Research International*[J], 2019, 26: 52

10 Feng R C, Yang S Z, Shao Z H *et al. Rare Metal Materials and Engineering*[J], 2022, 51(5): 1650

11 Yang S Z, Cao H, Liu Y *et al. Rare Metal Materials and Engineering*[J], 2022, 51(9): 3236

12 Lu K, Lu J. *Materials Science and Engineering A*[J], 2004, 375: 38

13 Liu G, Yong X P, Lu K. *China Surface Engineering*[J], 2001, 14: 5

14 Xiong T Y, Liu C W, Li Z C *et al. Materials Guide*[J], 2003, 17: 69

15 Ba D M, Ma S N, Li C Q *et al. Materials Engineering*[J], 2006, 12: 3

16 Wu Y L, Xiong Y, Chen Z G *et al. Materials Engineering*[J], 2021, 49: 137

17 Zhang X, Xiong Y, Chen Z G *et al. China Surface Engineering*[J], 2021, 34: 76

18 Chen H Y, Fu T L, Gao Y. *Surface Technology*[J], 2020, 49: 214

19 Cong J H, Wang L, Xu Y Z *et al. Rare Metal Materials and Engineering*[J], 2022, 51(1): 113

20 Qu S X, Wang G M, Zhou H F *et al. Computational Materials Science*[J], 2011, 50: 1567

21 Xu S Z, Chavoshi S Z, Su Y Q. *Physica Status Solidi RRL – Rapid Research Letters*[J], 2018, 12: 1

22 Liu L, Wang J, Gong S K *et al. Scientific Reports*[J], 2014, 4: 1

23 Gao Y J, Sun Y L, Yang Y B *et al. Molecular Simulation*[J], 2015, 41: 1546

24 Edalati K, Toh S, Iwaoka H *et al. Scripta Materialia*[J], 2012, 67: 814

25 An M R, Song H Y. *Science China Physics Mechanics & Astronomy*[J], 2013, 56: 1938

26 Forwood C T. *Philosophical Magazine A*[J], 2000, 80: 2747

27 Cao H, Rui Z Y, Chen W K *et al. Molecular Simulation*[J], 2018, 44: 1

28 Cao H, Chen W K, Rui Z Y *et al. Molecular Simulation*[J], 2022, 48: 231

29 Cao H, Rui Z Y, Chen W K *et al. Science China Technological Sciences*[J], 2019, 62: 1605

30 Wang H, Sun Y, Yang Z B *et al. The Chinese Journal of Nonferrous Metals*[J], 2022, 32(12): 3684 (in Chinese)

31 Zhao K, Wang M, Lin E X *et al. Rare Metal Materials and Engineering*[J], 2013, 42(10): 2048 (in Chinese)

32 Ovid'Ko I A, Sheinerman A G. *Reviews on Advanced Materials Science*[J], 2016, 44: 1

33 Lu L, Chen X H, Huang X X *et al. China Basic Science*[J], 2010, 12: 16

34 Thompson A P, Aktulga H M, Berger R *et al. Computer Physics Communications*[J], 2022, 271: 108 171

35 Mendelev M I, Underwood T L, Ackland G J. *Journal of Chemical Physics*[J], 2016, 145(15): 154 102

36 Faria B, Guarda C, Silvestre N *et al. Composites Part B: Engineering*[J], 2020, 187: 107 836

37 Zhang H, Ou X Q, Ni S *et al. Mechanics of Materials*[J], 2020, 151: 103 629

38 Stukowski A. *Modelling & Simulation in Materials Science & Engineering*[J], 2010, 18: 15 012

39 Tsuru T, Shibutani Y, Hirouchi T. *AIP Advances*[J], 2016, 6: 1

40 Goel S, Faisal N H, Luo X C *et al. Journal of Physics D-Applied Physics*[J], 2014, 47: 275 304

41 Song H Y, Sun Y. *Computational Materials Science*[J], 2015, 104: 46

42 Xue K M, Zhang Y Q, Wang L S *et al. The Chinese Journal of Nonferrous Metals*[J], 2021, 31(8): 2136 (in Chinese)

43 Zhang J, Feng R C, Yao Y J *et al. Materials Direct*[J], 2023, 37: 125

44 Wang H, Xu D S, Yang R. *The Chinese Journal of Nonferrous Metals*[J], 2010, 20(3): 457 (in Chinese)

45 Lu L, You Z S. *Journal of Metals*[J], 2014, 50: 129

46 Liu M P, Wang J, Jiang T H *et al. The Chinese Journal of Nonferrous Metals*[J], 2014, 24(6): 1383 (in Chinese)

47 Yu W S, Zhang L, Shen S P. *Journal of Solid Mechanics*[J], 2020, 41: 567

48 Cao A J, Wei Y G, Mao S X. *Applied Physics Letters*[J], 2007, 90: 151 909

孪晶界对TiAl合金超音速微粒轰击影响的分子动力学模拟

曹　卉[1,2]，杨文乐[1]，周宝成[1]，俞兆亮[1]，王靖淇[1]，李海燕[1,2]，刘俭辉[1,2]，冯瑞成[1,2]

(1. 兰州理工大学 机电工程学院，甘肃 兰州 730050)

(2. 兰州理工大学 数字制造技术与应用教育部重点实验室，甘肃 兰州 730050)

摘　要：TiAl合金因具有低密度、高比强度、高温抗氧化性等性能成为航空航天等领域最具潜力的高温轻质结构材料之一，但其具有本质脆性，在成型过程中易引入微裂纹、孔洞等缺陷，严重影响了其力学性能。超音速微粒轰击是新型表面改性技术之一，利用该技术研究了不同孪晶界数量和位置对TiAl合金力学性能和变形行为的影响。结果表明：不同孪晶界数量模型的屈服强度随孪晶界数量的增大而降低；孪晶界位置距模型上表面越近，材料屈服强度越低；随着孪晶界数量的增加，孪晶对位错运动的阻碍越明显，模型轰击后表面的塑性变形程度也越大，材料更易发生断裂；孪晶距离材料上表面越近，孪晶对位错生长的抑制越明显，进而影响材料强度；模型变形失效是位错与位错、位错与孪晶及其它缺陷共同作用的结果。

关键词：TiAl合金；超音速微粒轰击；孪晶界；分子动力学；力学性能

作者简介：曹　卉，女，1988年生，博士，讲师，兰州理工大学机电工程学院，甘肃 兰州 730050，电话：0931-5135199，E-mail：caoh@lut.edu.cn